Journal of Applied Fluid Mechanics, Vol. 12, No. 1, pp. 293-302, 2019.
Available online at www.jafmonline.net, ISSN 1735-3572, EISSN 1735-3645.
DOI: 10.29252/jafm.75.253.28960

Bluff Body Drag Control using Synthetic Jet

P. Gil

Rzeszow University of Technology, The Faculty of Mechanical Engineering and Aeronautics, Rzeszow, 35-959, al. Powstańców Warszawy 8, Poland

†*Corresponding Author Email: gilpawel@prz.edu.pl*

(Received March 7, 2018; accepted August 19, 2018)

ABSTRACT

The paper presents the results of an experimental investigation wherein the bullet form drag force as a function of oscillating actuator frequency, various voltage and for different orifice/slot configuration are studied. In order to perform the experiment, an axisymmetric bullet shape model with ellipsoidal nose was used in wind tunnel. The synthetic jet actuator was used to flow control at sharp cut end. The experiment was conducted in a wind tunnel with a working diameter of 1000 mm and a maximum velocity of 45 m/s. The measurements were carried out for the Reynolds number from 88000 to 352000 and for relatively large Strouhal numbers up to St = 4.5 based on model external diameter and free stream velocity. While synthetic jet was switched on, drag coefficient has been reduced by -6% and increased by +22% in relation to the case with the synthetic jet was switched off. The synthetic jet has more impact for relatively low free stream velocity and for single axisymmetric orifice.

Keywords: Synthetic jet; Zero-net-mass-flux; Drag; Bluff body; Bullet shaped body.

NOMENCLATURE

A	orifice total area
C_D	drag coefficient for synthetic jet on
C_{D0}	drag coefficient for synthetic jet off
d	orifice diameter
D	model external diameter
E_{rms}	output voltage from loudspeaker
F	drag force
f	excitation frequency
f_{vs}	frequency of vortex shedding
H	depth of cavity
L	model total length
p_d	dynamic pressure
P_{rms}	electrical power feeding a loudspeaker
Re	Reynolds number
St	Strouhal number
t	orifice thickness
U	free stream velocity
v	air kinematic viscosity

Other abbreviation

MO	multiple orifices
SJ	synthetic jet
SJA	synthetic jet actuator
SL	slot
SO	single orifice

1. INTRODUCTION

The long term increasing fuel prices and energy consumption has been a global issue. Fuel consumption due to aerodynamic drag of a road vehicle consumed more than half of the vehicle's energy at highway velocity (Krishnani (2009)).

Aerodynamic drag consists of two components: pressure drag and skin friction drag. Bluff body pressure drag accounts for more than 80% of the total drag and it is strongly dependent on body geometry due to boundary layer separation and formation of wake region behind the body (Sudin *et al.* (2014)). Reducing the aerodynamic drag improves fuel efficiency, thus shape optimization is an essential part of vehicle design process (Mayer & Wickern (2011); Kourta & Gilliéron (2009)).

Flow separation control can be divided into passive and active methods. The classification of both methods is based on the condition whether the energy is consumed to control the flow or not. Passive flow control consists of discrete obstacles like vortex generators VRs (Dubey *et al.* (2013); Koike *et al.* (2004); Gopal & Senthilkumar (2012); Kim & Chen (2010)), spoilers (Hu & Wong (2011)), diffusers (Huminic *et al.* (2012)) or other add-on devices (Wahba *et al.* (2012); Khalighi *et al.* (2013); Leder (1992); Soja (1994).

Active flow control includes steady jets, suction or unsteady jets see (Sudin *et al.* (2014); Littlewood & Passmore (2012); Rouméas *et al.* (2009); Zhang *et al.* (2008); Freud & Mungal (1994); Englar (2003); Geropp & Odenthal (2000); Tesař *et al.* (2016); Tounsi *et al.* (2016) and Kavousfar *et al.* (2016)).

Amitay *et al.* (1997) investigated flow separation on 2-D cylinder using spanwise pair of synthetic jet actuators. The experiments were conducted in an open return wind tunnel with square test section measuring 910 mm on the side. The maximum air velocity was 32 m/s. The cylindrical model was 62.2 mm diameter. The center section of the model was instrumented with a pair of adjacent plane synthetic jet actuator driven by piezoceramic discs. The cylindrical model can be rotated about its axis, thus the angle between the jets and the free stream can be varied. The cylinder was equipped with 47 pressure port around its circumference. Hot wire anemometry was used for streamwise velocity measurement and smoke visualization to demonstrate flow separation regime. Utilizing synthetic jet the cylinder drag force was reduced up to -30%.

Li *et al.* (2015) investigated drag control of a D-shaped bluff body using synthetic jet. A model made from acrylic glass was mounted in an open-loop wind tunnel with 300x300x700 mm test section. Two arrays of loudspeakers, 3 in each array were used to form two slot jets. Each slot of 2 mm height and 165 mm width were directed at 45° to the free stream and located along the upper and lower edges on the rear wall. Constant temperature anemometer was used to determine synthetic jet velocity and smoke wire visualization technique was used to study the evolution of the flow structure. Drag force with synthetic jet was reduced by -5% for actuating frequency about 2/3 of the natural shedding frequency. The largest increase in drag with synthetic jet was +18% for actuating frequency close to the natural shedding frequency.

Kourta & Leclerc (2013) studied Ahmed's body wake with synthetic jets. Experiments were conducted in the closed-loop wind tunnel with test section 2000x2000 mm and 5000 mm length. The maximum velocity reached 60 m/s. The generic car body with a rear slant angle of 25° scaled as 0.7 of the original Ahmed body. Inside the model were 10 piezoelectric synthetic jet actuators, which can be fitted at three different position: on the roof, the beginning of the rear window or on the rear window. Synthetic jet appears at slot with variable width from 0.5 mm to 2 mm. For body wake studied PIV measurement was employed. The maximum drag reduction was about -8.5%.

Pastoor *et al.* (2008) investigated experimentally drag reduction for the turbulent flow around D-shaped body. Experiments were conducted in open loop wind tunnel, with test section of 555 mm and 550 mm. The maximum velocity was 20 m/s with turbulence level less than 0.5%. Loudspeaker synthetic jet actuator with spanwise slots located at upper and lower trailing edges was used to flow control. The authors reached up to 40% base pressure increase associated with a -15% drag reduction employing synthetic jet.

Gao *et al.* (2016) studied effects of synthetic jets on a D-shaped cylinder wake. The cylinder wake was examined in detail based on flow visualization, pressure transducer and hot wire anemometer. Large scale vertical structures in the cylinder wake were modified by synthetic jet creating symmetric or asymmetric patterns. These observations were correlated with drag force variations.

Khalighi *et al.* (2001) investigated experimentally and computationally passive drag reduction device for bluff bodies. The square back model was installed in closed loop wind tunnel with rectangular test section with 711 mm width and 507 mm height. The experiment included PIV study, hot wire anemometry and pressure measurements. The device modified the flow field behind the model by disturbing the shear layer. The author reached -20% drag reduction by employing this passive device.

Aider *et al.* (2010) studied passive flow control on a 3D bluff body using vortex generators (VGs). The bluff body is a modified Ahmed body with curved rear part. The influence of a line of trapezoidal vortex generators in the drag and lift forces were investigated. The measurement was carried out in open wind tunnel with rectangular cross section 2100 mm high and 5200 mm wide. Maximum free stream velocity reached 40 m/s. For particular VRs configuration and location, the drag reduction reached -12%.

Drag control is very important issue in transport, due to fuel saving and reducing drive power. Despite the fact that bluff body drag control technique often causes drag increasing it can be also applied for e.g. braking or velocity control at constant drive power. The reduction of aerodynamic drag is possible both through active and passive methods.

Recently often used active method is synthetic jet produced by devices called zero net mass flux because the integration of the mass flow rate across the orifice or slot over an integer number of cycles is equal to zero. Synthetic jet actuator produce a train of vortex rings or pair which is in time-averaged senses produce a jet: Holman *et al.* (2005); Strzelczyk & Gil (2016) and Smyk (2017).

The aim of this work is to investigate the influence of the synthetic jet on bluff body drag. In particular, the influence of input voltage in range 3-6 V, actuation frequency from 0 to 350 Hz and different orifice/slot configuration has been tested. Synthetic jets exit was on the back plate of the bullet shaped body. A single axisymmetric orifice, multiple axisymmetric orifices, and a slot were tested. The aerodynamic drag, drag coefficient and pressure distribution in wake were measured with and without the synthetic jet. In previous studies, the influence of various methods on the aerodynamic drag has been investigated for relatively small Strouhal numbers: St < 0.35; see Li *et al.* (2015), and St < 0.4; see Gao *et al.* (2016). In this work this

range was extended up to St = 4.5.

2. EXPERIMENTAL SET-UP

The study was carried out in open-loop suction type wind tunnel located in Rzeszow University of Technology (Poland). The diameter of the measurement section is 1000 mm with a length of 1800 mm. The wind tunnel has a contraction ratio of 9. The fan is driven by a 90 kW DC motor with external cooling. The maximum free stream velocity reach 45 m/s with turbulence level less than 0.5%.

In order to perform the experiment, axisymmetric bullet shaped model was made. The skeleton of the model was made of aluminum, the housing was made of plexiglass tube, while the nose was made with ABS in rapid prototyping technology (Fig. 1). External diameter and total length were $D = 133$ mm and $L = 500$ mm respectively, so the ratio $L/D = 3.76$. The nose was geometrically half an ellipsoid with total length of 145 mm. The outer surface of the nose has been polished. Measurement were performed with a free-stream velocity of 10, 20, 30 and 40 m/s, the blockage ratio of test section was only 1.8%.

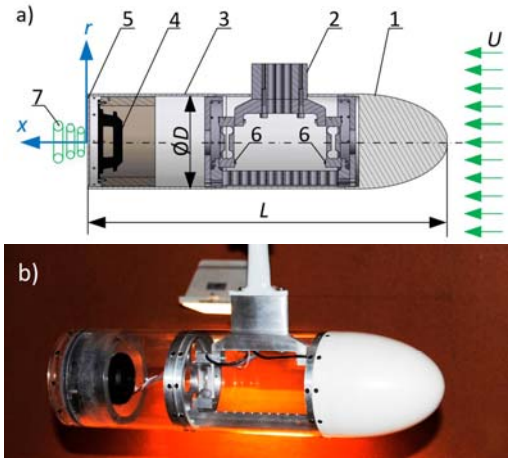

Fig. 1. a) Cross-section of the model: 1 – nose, 2 – fairing, 3 – plexiglass tube, 4 – synthetic jet actuator, 5 – back plate, 6 – load cells, 7 – synthetic jet b) photo of installed model in the wind tunnel.

Force measuring system consisted of two load cells installed inside model and connected with aluminum skeleton and fairing. The cross-section of the aluminum fairing was symmetrical airfoil. The fairing was attached to a steel pipe that is installed in the wind tunnel test section. Wires from SJA and load cells passed through the openings in the fairing and inside steel pipe. Between fairing and plexiglass tube small gap was made which enabled the model to move under drag force. The BTENS-N6 load cells with a maximum measuring range of 3 N were used.

Load cells were connected to the DBK 16 card, which was installed in DaqBook2000 series data acquisition system. The DBK 16 is two channel strain gage expansion card, enabling 16-bit, 200 kHz measurement. The gain and offset has been selected so that high signal values can be obtained for the considered range of drag measurement. Next the calibration was carried out. The calibration process consisted of loading the model by the line and the reel with the standard masses. Calibration was carried out at 20 points covering the entire measuring range from 0 to 5 N. The sampling frequencies of force measurement was 5 kHz and measurement time was 120 s. The relative uncertainty of the force measurement was estimated at 2%.

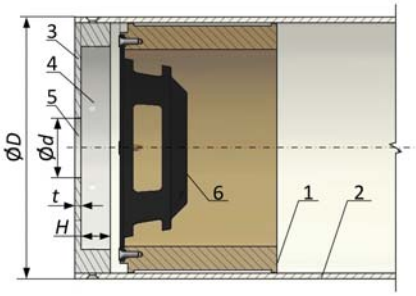

Fig. 2. Synthetic jet actuator: 1 – bushing, 2 – plexiglass tube, 3 – back plate, 4 – cavity, 5 – orifice/slot, 6 – loudspeaker.

At the back of the model synthetic jet actuator was installed. It consisted of an STX M.11.100.8.MC loudspeaker of 115 mm diameter fitted to a plexiglass bushing fixed and sealed in the model tube (Fig. 2). The loudspeaker nominal impedance is 8 Ω, measured resonance frequency is 90 Hz. In front of the loudspeaker diaphragm, a plexiglass plate (back plate) was mounted in which orifices or slot were located. Detailed geometries of the tested orifices/slot were presented in Fig. 3 and Table 1. Each plate had a thickness $t = 3$ mm.

Table 1. List of tested orifices

Type		Size	A [mm^2]	t [mm]
Single orifice	SO	Ø30	706	3
Multiple orifices	MO	9xØ10	706	3
Slot	SL	2xØ125	725	3

Total orifice/orifices or slot area is approximately equal $A = 706$ mm^2. Cavity depth is constant and is equal $H = 20$ mm. All orifices and slot has sharp edges.

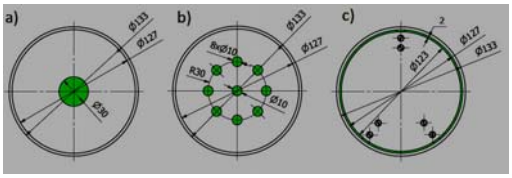

Fig. 3. Back plate, a) single axisymmetric orifice, b) multiple axisymmetric orifices, c) slot, (dimensions in mm).

SJA was powered by sinusoidal signal from function generator Rigol DG4062 and LM3886

Texas Instruments amplifier. The measurements included frequency range from 0 to 350 Hz, where 0 Hz means that synthetic jet was switched off. The root mean square voltage which powered the actuator, was maintained constant for particular set of experiments and was 3 V or 6 V. Multifunction board DBK80 was used for the purpose of continuous monitoring of the synthetic jet actuator voltage, current and frequency. The measurement of current in conjunction with voltage gave the electrical power supplied to the loudspeaker. The sampling frequency of electric measurements was 5 kHz and measurement time was 120 s. The relative uncertainty of the electrical measurement was estimated at 1%.

Free stream velocity in wind tunnel was measured with Prandtl tube connected to HCLA FIRSTSENSOR pressure transducer calibrated with FLUKE 718G pressure calibrator. The relative uncertainty of the velocity measurement was estimated at 2.5%. The sampling frequency of voltage signal from pressure transducer was 5 kHz and measurement time was 120 s.

Pressure distribution behind the model was measured with mini Prandtl tube connected to Honeywell XCAL4004GN pressure transducer with range ± 1250 Pa calibrated with FLUKE 718G pressure calibrator. The probe was installed on a three-axis manipulator with positioning accuracy of 0.1 mm. The relative uncertainty of the pressure measurement was estimated at 1.7%. The sampling frequencies of voltage signal from pressure transducer was 5 kHz and measurement time was 120 s. DASYLab routines was used for collecting all data from the DaqBook2000 system and saving in text files.

3. CALCULATION

The free stream Reynolds number is calculated as:

$$\mathrm{Re} = \frac{U \cdot D}{\nu} \tag{1}$$

The Strouhal number is defined as:

$$\mathrm{St} = \frac{f \cdot D}{U} \tag{2}$$

The drag coefficient is defined as:

$$\mathrm{C_D} = \frac{F}{p_d \cdot \frac{\pi}{4} \cdot D^2} \tag{3}$$

The experiment was carried out in accordance with Table 2. A total of 24 cases were tested for three different orifices/slot geometries.

4. RESULTS

4.1 Shedding Frequency

The bullet-shaped body is a bluff body, and so a vortex shedding takes place at the rear sharp edge. Due to vortex shedding, the model starts vibrating. Instantaneous drag force for various free stream velocity is presented in Fig. 4, and (for comparison purposes) instantaneous free stream velocity is presented in Fig. 5.

Table 2 Parameter settings

Name		U [m/s]	E_{rms} [V]	f [Hz]
Case 1	SO	10	3	0-350
Case 2	SO	20	3	0-350
Case 3	SO	30	3	0-350
Case 4	SO	40	3	0-350
Case 5	SO	10	6	0-350
Case 6	SO	20	6	0-350
Case 7	SO	30	6	0-350
Case 8	SO	40	6	0-350
Case 9	MO	10	3	0-350
Case 10	MO	20	3	0-350
Case 11	MO	30	3	0-350
Case 12	MO	40	3	0-350
Case 13	MO	10	6	0-350
Case 14	MO	20	6	0-350
Case 15	MO	30	6	0-350
Case 16	MO	40	6	0-350
Case 17	SL	10	3	0-350
Case 18	SL	20	3	0-350
Case 19	SL	30	3	0-350
Case 20	SL	40	3	0-350
Case 21	SL	10	6	0-350
Case 22	SL	20	6	0-350
Case 23	SL	30	6	0-350
Case 24	SL	40	6	0-350

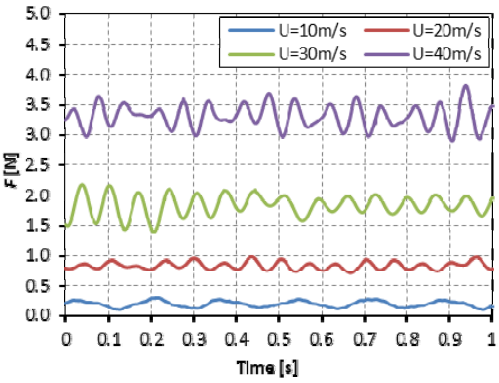

Fig. 4. Instantaneous drag (SJ – off).

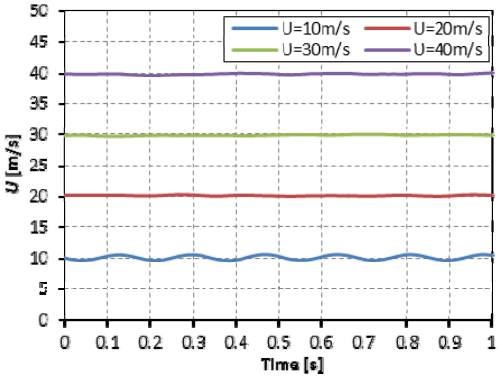

Fig. 5. Instantaneous free stream velocity.

The instantaneous free stream velocity for 20, 30 and 40 m/s is almost constant, only for 10 m/s it

shows some low-frequency pulsations which results from the wind tunnel's constructional compliance.

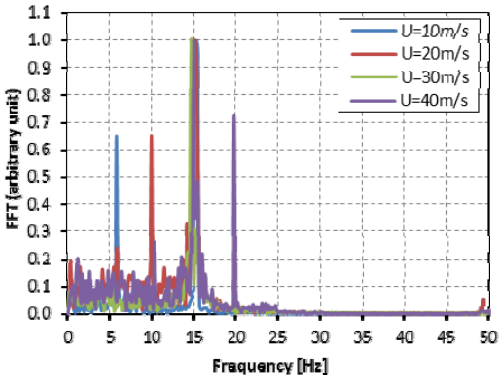

Fig. 6. Fast Fourier transform FFT (SJ – off).

By applying fast Fourier transform of load cells signal, characteristic frequency can be obtained (Fig. 6). There are two frequency peaks for each velocity. First peak remains constant and corresponds to the body natural frequency. The second peaks vary due to vortex shedding frequency (Fig. 7). Bullet shaped body natural frequency is 15.3 Hz.

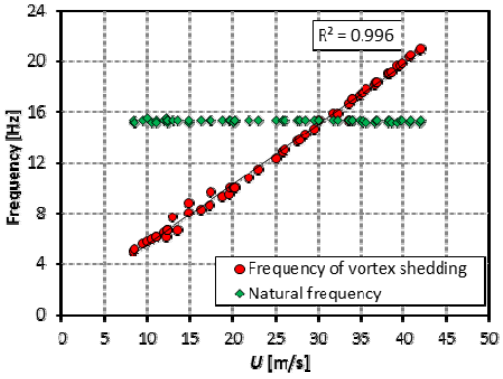

Fig. 7. The vortex shedding frequency as a function of free stream velocity (SJ – off).

The vortex shedding frequency is f_{vs} = 5.8Hz for U = 10 m/s and f_{vs} = 19.7 Hz for U = 40 m/s. As the free stream velocity increases, the vortex frequency increases linearly as well. For free stream velocity U = 32 m/s the vortex shedding frequency is about f_{vs} = 15 Hz and reaches the natural frequency of the model what causes vortex-induced vibration (Marris (1964); Williamson & Govardhan (2004)). The vortex-induced vibration causes a significant increase in the model amplitude of vibrations.

Calculating the Strouhal number for vortex shedding frequencies with synthetic jet switched off, St* = 0.07 can be obtained which compares well with literature values for similar flows: Khalighi *et al.* (2013), Lanser *et al.* (1991), Bearman (1967).

4.2 Drag Coefficient

The bluff body drag depends on air density, free stream velocity, shape and orientation of the body.

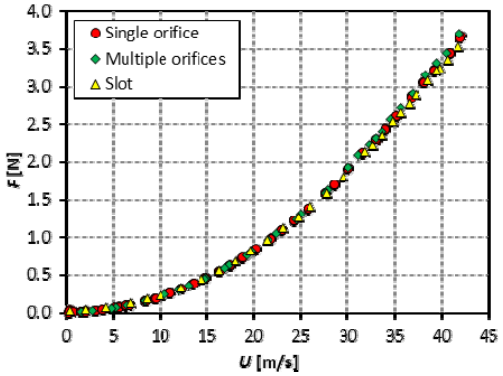

Fig. 8. Drag versus free stream velocity (SJ – off).

The drag versus free stream velocity, when synthetic jet is switched off, is presented in Fig. 8 for different orifices/slots. As can be seen in this figure, after installing the new plate with the orifices/slot and after starting a new series of measurements, the results coincide. The measured drag is relatively small, for U = 40 m/s reaches F = 3.4 N.

Instead of drag, it is convenient to operate with drag coefficient. Drag coefficient as a function of Reynolds number for synthetic jet switched off is presented in Fig. 9.

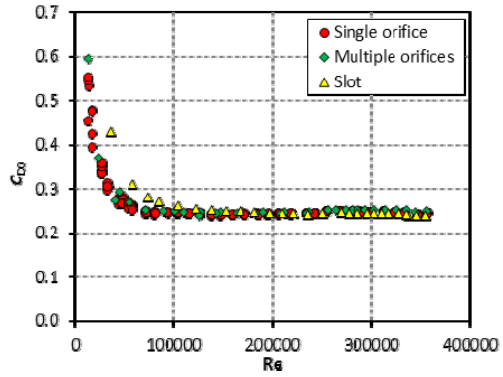

Fig. 9. Drag coefficient as a function of Reynolds number (SJ – off).

For Reynolds number less than 50000 the drag coefficient increases rapidly up to C_{D0} = 0.6 for Re = 13300 witch is in good agreement with data for laminar flow presented by Jiménez-González *et al.* (2013). For Reynolds number from Re = 100000 up to Re = 350000 the drag coefficient is almost constant C_{D0} = 0.24.

4.3 SJA Power Consumption

Active drag control, in contrast to passive drag control, requires energy supply. Synthetic jet actuator is powered by electricity. Electrical power feeding a loudspeaker for three different orifices/slot geometries and for two power supply voltage is presented in Fig. 10.

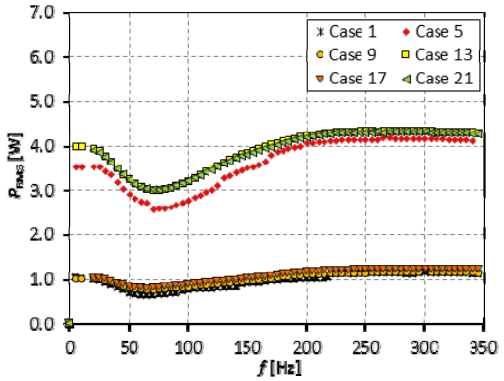

Fig. 10. Electrical power feeding SJA.

The local minimum informs about the loudspeaker resonant frequency working in plexiglass chamber. This frequency is around 70 Hz. Lower power consumed by synthetic jet actuator for single orifice (SO, case 1 and case 5) results from the smallest hydraulic diameter with all investigated cases.

4.4 Single Orifice

This subsection presents the results of using single axisymmetric synthetic jet to bluff body flow control. Instead of drag coefficient, it is convenient to work with the ratio of drag coefficient with synthetic jet switched on to drag coefficient with synthetic jet switched off, i.e., C_D/C_{D0}. Drag coefficient ratio versus frequency for 1-8 cases are presented in Fig. 11. The C_D/C_{D0} ratios reach local maximum or minimum close to SJA resonance frequency 70 Hz. Reduced drag coefficient versus Strouhal number is presented in Fig. 12.

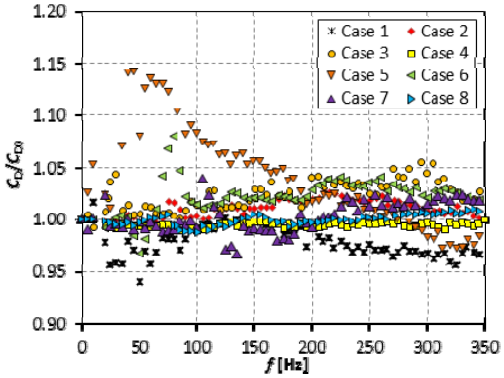

Fig. 11. Drag coefficient ratio versus frequency, (SJ – on).

The C_D/C_{D0} ratio deviates from unity especially for low velocity (case 1 and case 5). If the free stream velocity is higher, the impact of the synthetic jet is smaller (case 4 and case 8). The vortex shedding reduced frequencies from bullet shaped body is about St* = 0.07, for synthetic jet on, maximum C_D/C_{D0} ratios appear close to St = 0.7 or St = 1.4 whereas the minimum value appears close to St = 0.7 or St = 4.2.

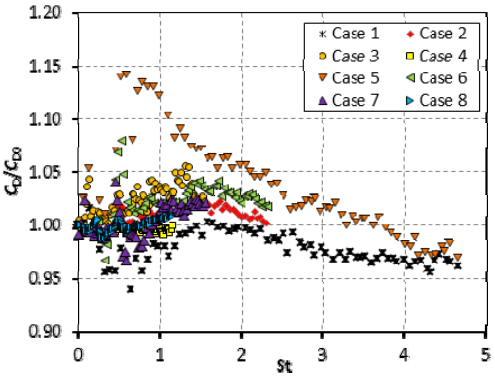

Fig. 12. Drag coefficient ratio versus Strouhal number (SJ – on).

For free stream velocity 10 m/s maximum reduction of drag coefficient -6% occurs at St = 0.64 and E_{rms} = 3 V, while the maximum increase of drag coefficient +14% occurs at St = 0.7 and E_{rms} = 6 V. For the highest tested velocity 40 m/s maximum reduction of drag coefficient -1.2% occurs at St = 0.58 and E_{rms} = 3 V, while the maximum increase of drag coefficient +1.1% occurs at St = 0.8 and E_{rms} = 6V.

As mentioned previously, for free stream velocity U = 32 m/s, which is close to U = 30 m/s (case 3 and case 7), vortex-induced vibration takes place, however, the measured data for this cases does not give a significant discrepancy in relation to other cases.

4.5 Multiple Orifices

This subsection presents the results of using multiple axisymmetric synthetic jets to bluff body flow control. Drag coefficient ratio versus frequency is presented in Fig. 13. The C_D/C_{D0} ratios reach local maximum close to 110 Hz. Drag coefficient ratio versus Strouhal number is presented in Fig. 14.

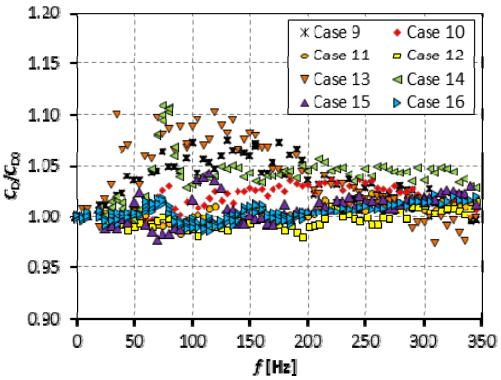

Fig. 13. Drag coefficient ratio versus frequency, (SJ – on).

For synthetic jet on, maximum C_D/C_{D0} ratios appear close to St = 0.5 or St = 1.5 whereas the minimum value appears close to St = 0.4 or St = 4.2.

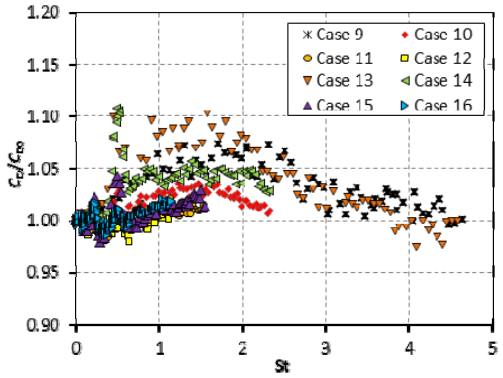

Fig. 14. Drag coefficient ratio versus Strouhal number (SJ – on).

For free stream velocity 10 m/s maximum reduction of drag coefficient -2.6% occurs at St = 4.1 and E_{rms} = 6 V, while the maximum increase of drag coefficient +10.2% occurs at St = 0.5 and E_{rms} = 6 V. For the highest tested velocity 40 m/s maximum reduction of drag coefficient -2% occurs at St = 0.64 and E_{rms} = 3 V, while the maximum increase of drag coefficient +2.1% occurs at St = 1.1 and E_{rms} = 6 V.

4.6 Slot

This subsection presents the results of using slot emanating synthetic jets to bluff body flow control. Drag coefficient ratio versus frequency is presented in Fig. 15. The C_D/C_{D0} ratios reach local maximum close to 50-70 Hz. Reduced drag coefficient versus Strouhal number is presented in Fig. 16.

For synthetic jet on, maximum C_D/C_{D0} ratio is close to St = 0.5 whereas the minimum value appears close to St = 0.25 or St = 4.5. For free stream velocity 10 m/s maximum reduction of drag coefficient -3.9% occurs at St = 4.6 and E_{rms} = 6 V, while the maximum increase of drag coefficient +19% occurs at St = 0.46 and E_{rms} = 6 V.

For the highest tested velocity 40 m/s maximum reduction of drag coefficient -1.9% occurs at St = 0.25 and E_{rms} = 6 V, while the maximum increase of drag coefficient +3.9% occurs at St = 0.5 and E_{rms} = 6 V.

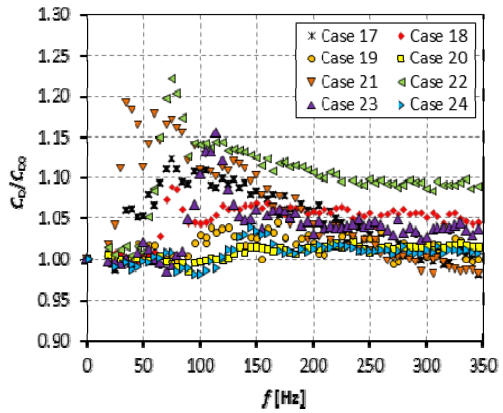

Fig. 15. Reduced drag coefficient versus frequency (SJ – on).

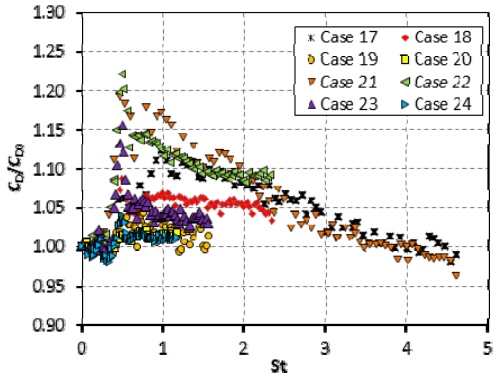

Fig. 16. Reduced drag coefficient versus Strouhal number (SJ – on).

4.7 Pressure Distribution

The dynamic pressure distributions are presented in Figs. 17 and 18 for free stream velocity U = 40 m/s and U = 10 m/s respectively. For the highest tested velocity, dynamic pressure reaches p_d = 1000 Pa, while for the lowest tested velocity reaches p_d = 63 Pa. Pressure profiles were collected in the axial distance from x = 26 mm to x = 532 mm (x/D = 0.2 to x/D = 4) and from radial coordinate r = -133 mm to r = 133 mm (r/D = -1 to r/D = 1).

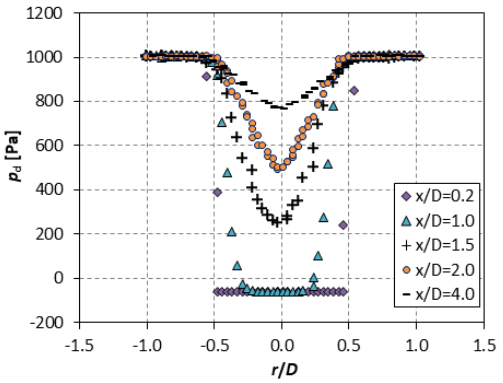

Fig. 17. Pressure distribution behind model for U = 40 m/s, (SJ – off).

Pressure drag dominates total drag in bluff body. The under-pressure appears just behind the back plate under normal air flow and for synthetic jet switched off. For flow U = 40 m/s the under-pressure reaches up to -60 Pa, while for U = 10 m/s it reaches -12 Pa. From Figs. 17 and 18 it can be seen that along with increasing distances from the model, pressure recovery takes place. The aerodynamic drag arises from separated flows, causing pressure recovery losses and generation of vorticity in the wake. Synthetic jet allows to modify the pressure field in the wake, which can change the total body drag.

In Fig. 19 a comparison of pressure distributions was presented in far filed (x/D = 4) for synthetic jet switched off and syntehtic jet switched on, case 7, f = 130Hz. In this case drag reduction was -2.6%. From Fig. 19 it can be seen that the maximum pressure deficit in far wake decreases by about

50 Pa, but the width of the wake is increased. Modification of the aerodynamic wake with a synthetic jet gives rise to a decrease or increase in the pressure distribution which results in pressure drag change.

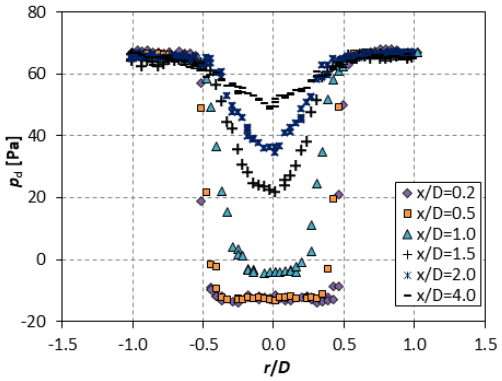

Fig. 18. Pressure distribution behind model for U = 10 m/s (SJ – off).

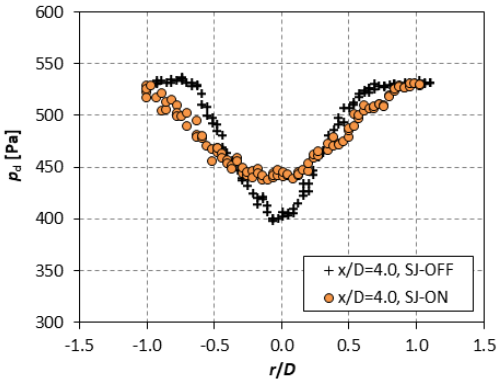

Fig. 19. Pressure distribution for U = 30 m/s, SJ-off and SJ-on (Case 7, f = 130 Hz).

5. DISCUSSION

The drag coefficient ratio versus free stream velocity for all cases is presented in Fig. 20. The graph presents all measurement data for maximum and minimum C_D/C_{D0} ratio values. The experiments show that, as the free stream velocity (or, equivalently, the Reynolds number) increases, the effectivity of synthetic jet on drag control decreases.

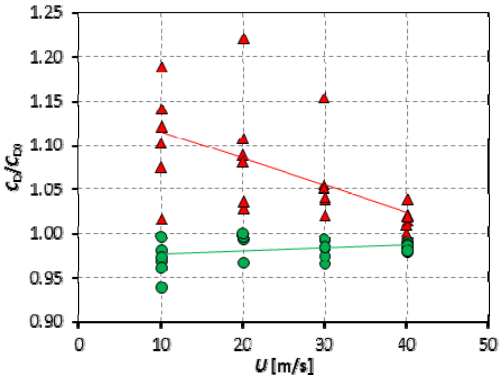

Fig. 20. Reduced drag coefficient versus free stream velocity.

The reduced drag coefficient versus free stream velocity for different orifices/slot geometries is presented in Fig. 21.

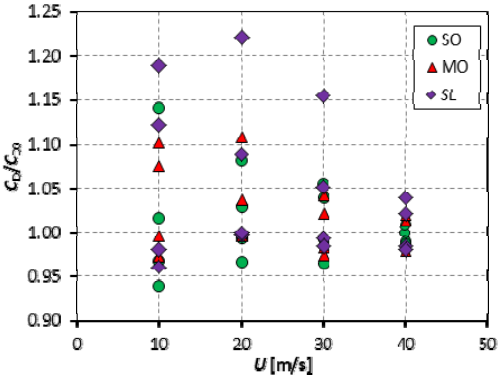

Fig. 21. Reduced drag coefficient versus free stream velocity for different geometry.

The highest drag reduction is achieved for single orifice (SO), despite the fact that the hole is farthest from the sharp edge. However, for the slot, which is close to the sharp edge, less drag reduction is obtained. Moreover, for some parameters the highest drag increase is obtained.

Drag coefficient ratio versus free stream velocity for different voltage is presented in Fig. 22. With increasing synthetic jet actuator supply voltage, momentum velocity increases, what was presented by Gil & Strzelczyk (2016). Therefore, as the voltage increases, the impact of a synthetic jet on the drag control increases.

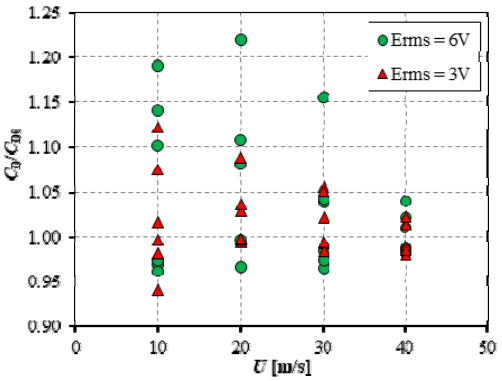

Fig. 22. Reduced drag coefficient versus free stream velocity for different voltage.

The synthetic jet actuator causes the reaction force, which decreases the drag force, however this situation takes place only when the SJA has a configuration as presented in Fig. 1. In this study the resolution of force measurement prevented accurate measurement of this forces but Trávníček *et al.* (2005), Trávníček *et al.* (2008) and Gil (2018) investigated experimentally SJA force and obtained maximum 10-35 mN. This result was obtained in an undisturbed field, whereas in this case there is an external air flow close to SJA.

6. CONCLUSION

The use of synthetic jet for active control of drag is promising. Experimental measurement were carried out to find out the relationship between orifice/slot geometry, SJA signal frequency, voltage and free stream velocity on decreasing or increasing drag. The measurements were carried out for the Reynolds number from 88000 to 352000 based on bullet external diameter and free stream velocity. During synthetic jet on, drag coefficient was reduced by about -6% and increased by about +22% in relation to the case with the synthetic jet off. The synthetic jet has more impact for relatively low free stream velocity. For single orifice, the largest drag reduction was obtained, while for slot the largest drag increase was obtained.

REFERENCES

Aider, J. L., J. F. Beaudoin and J. E. Wesfreid (2010). Drag and lift reduction of a 3D bluff-body using active vortex generators. *Experiments in fluids* 48 (5), 771-789.

Amitay, M., A. Honohan, M. Trautman and A. Glezer (1997). Modification of the aerodynamic characteristics of bluff bodies using fluidic actuators. *In 28th Fluid Dynamics Conference*, (p. 2004).

Bearman, P. W. (1967). The effect of base bleed on the flow behind a two-dimensional model with a blunt trailing edge. *The Aeronautical Quarterly* 18 (3), 207-224.

Dubey, A., S. Chheniya and A. Jadhav (2013). Effect of Vortex generators on Aerodynamics of a Car: CFD Analysis. *International Journal of Innovations in Engineering and Technology* 2 (1), 137-144.

Englar, R. J. (2003). Drag reduction, safety enhancement, and performance improvement for heavy vehicles and SUVs using advanced pneumatic aerodynamic technology (No. 2003-01-3378). *SAE Technical Paper*.

Freund, J. B. and M. G. Mungal (1994). Drag and wake modification of axisymmetric bluff bodies using Coanda blowing. *Journal of Aircraft* 31(3), 572-578.

Gao, N., Y. Q. Li, H. L. Bai and C. J. Wu (2016). Effects of Synthetic jets on a D-Shaped Cylinder wake at a Subcritical Reynolds Number. *Flow Turbulence and Combustion* 97 (3), 729-742.

Geropp, D. and H. J. Odenthal (2000). Drag reduction of motor vehicles by active flow control using the Coanda effect. *Experiments in fluids* 28(1), 74-85.

Gil, P. (2018). Synthetic jet Reynolds number based on reaction force measurement. *Journal of Fluids and Structures* 81, 466-478

Gil, P. and P. Strzelczyk (2016). Performance and efficiency of loudspeaker driven synthetic jet actuator. *Experimental Thermal and Fluid Science* 76, 163-174.

Gopal, P. and T. Senthilkumar (2012). Aerodynamic drag reduction in a passenger vehicle using vortex generator with varying yaw angles. *ARPN Journal of Engineering and Applied Sciences* 7 (9), 1180-1184.

Holman, R., Y. Utturkar, R. Mittal, B. L. Smith and L. Cattafesta (2005). Formation criterion for synthetic jets. *AIAA J*. 43 (10), 2110–2116.

Hu, X. X. and T. T. Wong (2011). A numerical study on rear-spoiler of passenger vehicle, World Academy of Science, *Engineering and technology* 57, 636-641.

Huminic, A., G. Huminic and A. Soica (2012). Study of aerodynamics for a simplified car model with the underbody shaped as a venturi nozzle. *International Journal of Vehicle Design* 58 (1), 15-32.

Jiménez-González, J. I., E. Sanmiguel-Rojas, A. Sevilla and C. Martínez-Bazán (2013). Laminar flow past a spinning bullet-shaped body at moderate angular velocities. *Journal of Fluids and Structures* 43, 200-219.

Kavousfar, S., E. Esmaeilzadeh, H. Mahdavy-Moghaddam, M. Mirzaei and S. G. Pouryoussefi (2016). Experimental Study of Plasma Actuator Effects on Flow Field Separation Bubble around Blunt Flat Plate. *Journal of Applied Fluid Mechanics* 9 (1), 397-406.

Khalighi, B., S. R. Balkanyi and L. P. Bernal (2013). Experimental investigation of aerodynamic flow over a bluff body in ground proximity with drag reduction devices. *International Journal of Aerodynamics* 3 (4), 217-233.

Khalighi, B., S. Zhang, C. Koromilas, S. R. Balkanyi, L. P. Bernal, G. laccarino, P. Moin (2001). Experimental and computational study of unsteady wake flow behind a bluff body with a drag reduction device. *SAE Technical Paper*, (No. 2001-01-1042).

Kim, I. and H. Chen (2010). Reduction of aerodynamic forces on a minivan by a pair of vortex generators of a pocket type. *International journal of vehicle design* 53 (4), 300-316.

Koike, M., T. Nagayoshi and N. Hamamoto (2004). Research on aerodynamic drag reduction by VGs. *Mitshubishi Motors Technical Review* 16, 11-16.

Kourta, A. and P. Gilliéron (2009). Impact of the automotive aerodynamic control on the economic issues. *Journal of Applied Fluid Mechanics* 2 (2), 69-75.

Kourta, A. and C. Leclerc (2013). Characterization of synthetic jet actuation with application to Ahmed body wake. *Sensors and Actuators A: Physical* 192, 13-26.

Krishnani, P. N. (2009). *CFD study of drag reduction of a generic sport utility vehicle*. Master's Thesis, Mechanical Engineering Department, California State University, Sacramento.

Lanser, W. R., J. C. Ross and A. E. Kaufman (1991). Aerodynamic performance of a drag reduction device on a full-scale tractor/trailer. *SAE Technical Paper*, (No. 912125).

Leder, A. (1992). Abgelöste Strömungen Physikalische Grundlagen. Vieweg + Teubner, Wiesbaden, DE.

Li, Y., H. Bai and N. Gao (2015). Drag of a D-shaped bluff body under small amplitude harmonic actuation. *Theoretical and Applied Mechanics Letters* 5 (1), 35-38.

Littlewood, R. P. and M. A. Passmore (2012). Aerodynamic drag reduction of a simplified squareback vehicle using steady blowing. *Experiments in fluids* 53 (2), 519-529.

Marris, A. W. (1964). A review on vortex streets, periodic wakes, and induced vibration phenomena. *Journal of Basic Engineering* 86(2), 185-193.

Mayer, W. and G. Wickern (2011). The new Audi A6/A7 family aerodynamic development of different body types on one platform. *SAE International Journal of Passenger Cars-Mechanical Systems* 4 (1), 197-206.

Pastoor, M., L. Henning, B. R. Noack, R. King and G. Tadmor (2008). Feedback shear layer control for bluff body drag reduction. *Journal of Fluid Mechanics* 608, 161-196.

Rouméas, M., P. Gilliéron and A. Kourta (2009). Drag reduction by flow separation control on a car after body. *International Journal for Numerical Methods in Fluids* 60 (11), 1222-1240.

Smyk, E. (2017). Interference in axisymmetric synthetic jet actuator. *In EPJ Web of Conferences* (Vol. 143, p. 02111). EDP Sciences.

Soja, H., 1994. Beeinflussung des Hecktotwassers an Fahrzeugkörpern in Bodennähe und dessen Auswirkung auf die aerodynamischen Beiwerte. Dissertation, Universität Stuttgart, Stuttgart, German.

Strzelczyk, P. and P. Gil (2016). Properties of velocity field in the vicinity of synthetic jet generator. In *Journal of Physics: Conference Series*. 760(1).

Sudin, M. N., M. A. Abdullah, S. A. Shamsuddin, F. R. Ramli and M. Mohd (2014). Review of research on vehicles aerodynamic drag reduction methods. *International Journal of Mechanical and Mechatronics Engineering* 14 (2), 35-47.

Tesař, V., K. Peszynski and E. Smyk (2016). Fluidic low-frequency oscillator consisting of load-switched diverter and a pair of vortex chambers. *In EPJ Web of Conferences* (Vol. 114, p. 02121). EDP Sciences.

Tounsi, N., R. Mestiri, L. Keirsbulck, H. Oualli, S. Hanchi and F. Aloui (2016). Experimental Study of Flow Control on Bluff Body using Piezoelectric Actuators. *Journal of Applied Fluid Mechanics* 9 (2), 827-838.

Trávníček, Z., A. I. Fedorchenko and A. B. Wang (2005). Enhancement of synthetic jets by means of an integrated valve-less pump: part I. Design of the actuator. *Sensors and Actuators A: Physical* 120(1), 232-240.

Trávníček, Z., V. Tesař and J. Kordík (2008). Performance of synthetic jet actuators based on hybrid and double-acting principles. *Journal of Visualization* 11(3), 221-229.

Wahba, E., H. Al-Marzooqi, M. Shaath, M. Shahin and T. ElDhmashawy (2012). Aerodynamic drag reduction for ground vehicles using lateral guide vanes. *CFD Letters* 4 (2), 68-79.

Williamson, C. H. K. and R. Govardhan (2004). Vortex-induced vibrations. *Annual Review of Fluid Mechanics* 36, 413-455.

Zhang, P., J. Wang and L. Feng (2008). Review of zero-net-mass-flux jet and its application in separation flow control. *Science in China series E: technological sciences* 51 (9), 1315-1344.